Evaluating the Portability of Satellite Derived Chlorophyll-a Algorithms for Temperate Inland Lakes using Airborne Hyperspectral Imagery and Dense Surface Observations

Authors: Richard Johansen* [a], Richard Beck [a], Jakub Nowosad [a], Christopher Nietch [e] Min Xu [a], Song Shu [a], Bo Yang [a], Hongxing Liu [a], Erich Emery [b], Molly Reif [c], Joseph Harwood [c], Jade Young [d], Dana Macke [e], Mark Martin [f], Garrett Stillings [f], Richard Stumpf [g], Haibin Su [h]

[a] Department of Geography and GIS, University of Cincinnati, Cincinnati, OH 45221, USA
[b] U.S. Army Corps of Engineers, Great Lakes and Ohio River Division, Cincinnati, OH, 13 45202, USA
[c] U.S. Army Corps of Engineers, ERDC, JALBTCX, Kiln, MS 39556, USA
[d] U.S. Army Corps of Engineers, Louisville District, Water Quality, Louisville, KY 40202, USA
[e] U.S. Environmental Protection Agency, Cincinnati, OH 45268, USA
[f] Kentucky Department of Environmental Protection, Division of Water, Frankfort, KY 40601, USA
[g] National Oceanic and Atmospheric Administration, National Ocean Service, Silver Spring, MD, USA
[h] 22 Department of Physics and Geosciences, Texas A&M Kingsville, Kingsville, TX, 23 78363-8202, USA

** Corresponding Author*
E-Mail addresses: johansra@mail.uc.edu *(R. Johansen),* richard.beck@uc.edu *(R.A. Beck),* nowosad.jakub@gmail.com *(J. Nowosad),* nietch.christopher@epa.gov *(C.T. Nietch),* xum4@mail.uc.edu *(Min. X.),* shusg@mail.uc.edu *(Shu, S.),* yangb2@mail.uc.edu *(Bo.Y.),* hongxing.liu@uc.edu *(Hongxing, L.),* erich.b.emery@usace.army.mil *(E.B.Emery),* molly.k.reif@usace.army.mil *(M.K. Reif);* joseph.h.harwood@usace.army.mil *(J.H.Harwood),* jade.l.young@usace.army.mil *(J.L.Young),* macke.dana@epa.gov *(D. Macke),* mark.martin@ky.gov *(M. Martin),* garrett.stillings@ky.gov *(G. Stillings),* richard.stumpf@noaa.gov *(R. Stumpf),* haibin.su@tamuk.edu *(H. Su)*

Abstract:

This study evaluated the performances of twenty-nine algorithms that use satellite-based spectral imager data to derive estimates of chlorophyll-a concentrations that, in turn, can be used as an indicator of the general status of algal cell densities and the potential for a harmful algal bloom (HAB). The performance assessment was based on making relative comparisons between two temperate inland lakes: Harsha Lake ($7.99 km^2$) in Southwest Ohio and Taylorsville Lake ($11.88 km^2$) in central Kentucky. Of interest was identifying algorithm-imager combinations that had high correlation with coincident chlorophyll-a surface observations for both lakes, as this suggests portability for regional HAB monitoring. The spectral data utilized to estimate surface water chlorophyll-a concentrations were derived from the airborne Compact Airborne Spectral Imager (CASI) 1500 hyperspectral imager, that was then used to derive synthetic versions of currently operational satellite-based imagers using spatial resampling and spectral binning. The synthetic data mimics the configurations of spectral imagers on current satellites in earth's orbit including, WorldView-2/3, Sentinel-2, Landsat-8, Moderate-resolution Imaging Spectroradiometer (MODIS), and Medium Resolution Imaging Spectrometer (MERIS). High correlations were found between the direct measurement and the imagery-estimated chlorophyll-a concentrations at both lakes. The results determined that eleven out of the twenty-nine algorithms were considered portable, with r^2 values greater than 0.5 for both lakes. Even though the two lakes are different in terms of background water quality, size and shape, with Taylorsville being generally less impaired, larger, but much narrower throughout, the results support the portability of utilizing a suite of certain algorithms across multiple sensors to detect potential algal blooms through the use of chlorophyll-a as a proxy. Furthermore, the strong performance of the Sentinel-2 algorithms is exceptionally promising, due to the recent launch of the second satellite in the constellation, which will provide higher temporal resolution for temperate inland water bodies. Additionally, scripts were written for the open source statistical software R that automate much of the spectral data processing steps. This allows for the simultaneous consideration of numerous algorithms across multiple imagers over an expedited timeframe for the near real-time monitoring required for detecting algal blooms and mitigating their adverse impacts.

Keywords: Chlorophyll-a; Algal Bloom, Hyperspectral, Algorithms, Temperate Lakes

1. Introduction:

Over the last several decades, there has been a noticeable increase in the frequency and extent of freshwater harmful and algal blooms (HABs) in the United States (Reif ,2011; USEPA, 2012). Exact environmental mechanisms have yet to be determined (Graham, 2006; Linkov, Satterstrom, Loney, & Steevans, 2009), although, high nutrient concentrations and algae available insolation appear to be significant contributing factors (Dokulil and Teubner, 2000; Ohio EPA, 2012). Freshwater HNABs have become a global concern affecting forty-five countries worldwide and have resulted in animal deaths in at least twenty-seven US states (Graham, 2006, USEPA, 2012; WHO, 2003). What makes these blooms "harmful" is that the algae comprising the bloom can produce toxic compounds including, dermatoxins, hepatoxins, and neurotoxins dangerous to both humans and animals (USEPA, 2012). Although the World Health Organization and state agencies such as, the Ohio Department of Health, have set safety standards for the consumption and contact of these toxins (ODH 2017), their monitoring in small to mid-sized water bodies is difficult, time intensive, and costly (Backer, 2002; Pitois et., 2000). Remote sensing using satellite imagers for the detection of HNABs is possible because of photo reactive pigments produced by algae. These pigments have reflective properties that can be 'sensed' by analyzing the images. The toxins produced by algae are not directly detectable by the imagery, but toxin concentration is often correlated with algal biomass density, which in turn, is directly related to the concentration of photopigments (Gitelson et al., 1986; Gitelson et al., 2003; Kudela et al., 2015; Morel and Prieur, 1997; Stumpf et al., 2012; Stumpf et al. 2016; Vos et al., 1986; Wynne et al., 2012). One of the most abundant photopigments produced by all types of algae is chlorophyll-a, which is detectable by satellite imagery, therefore, can serve as an indicator of the presence of an algal bloom (Morel & Prieur, 1977; Vos, Donze, & Bueteveld, 1986; Gitelson, Nikanorov, Sabo, & Szilagyi, 1986; Gitelson, Gritz, & Merzlyak, 2003; Wynne, Stumpf, Tomlinson, & Dyble, 2012; Stumpf, Wynne, Baker, & Fahnenstiel, 2012; Kudela et al., 2015) and is a reliable proxy for water quality (Verdin, 1985; Ekstrand, 1992; Reif, 2011; Mishra & Mishra, 2012). So, while satellite imagery allows for remote sensing of a proxy for algal density, subsequent water sampling for toxin analysis would still be necessary to validate a high signal from the satellite and to evaluate the nature of the bloom to determine toxicity.

To reduce costs and increase coverage of algal bloom monitoring the use of remote sensing, especially from satellite platforms, are currently being utilized to address the risk management challenges associated with HNABs including, the monitoring of smaller fresh water lakes, rivers, and reservoirs, long-term studies of individual bodies of water, and the development of techniques for early detection (Shen, Xu, & Guo, 2012). The most effective way to accomplish these goals are through the continual use of high temporal resolution satellites with spatial resolutions significantly less than the size of the water body being observed (Beck et al. 2016). Temporal resolution is of the utmost importance, especially in temperate regions where freshwater HABs typically occur during the summer, corresponding to the most frequent chances of heavy cloud cover which can influences satellite imager's effectiveness. Therefore, the ability to maximize the number of satellites to image algal blooms in inland water bodies is important (Veryla, 1995). Ideal remote imaging systems would allow for quicker turnaround time for water safety officials to notify the public about potential HAB occurrence (Blondeau-Patissier, Gower, Dekker, Phinn, & Brando, 2014; Klemas, 2012; Stumpf & Tomlinson, 2005).

There has been some success in the global monitoring of algal blooms using satellites systems with high return times and swath widths of sensors such as the Moderate Resolution Imaging Spectroradiometer (MODIS), Ocean and Land Colour Instrument (OLCI) or the Medium Resolution Imaging Spectrometer (MERIS) (Augusto-Silva et al., 2014; Blondeau-Patissier et al., 2014; Klemas, 2012; Stumpf et al., 2012). Since MERIS is no longer operational, the similarly configured sensor, OLCI on the European Space

Agency's (ESA) Sentinel-3, takes MERIS's place for data after the launch date of February 16th, 2016 (ESA, 2018). Unfortunately, these imagers are less useful for the monitoring of small to mid-sized inland lakes that typically have widths of less than a few kilometers. Satellites with better spatial resolution typically have too long return times to monitor HNABs whose growth dynamics in surface waters may have sub-daily response times (Hunter et al, 2005). Beck et al. (2016) suggested the use of a suite of sensors in order to optimize the successful acquisition of a cloud-free scene and provide effective monitoring of small freshwater lakes for minimal cost. This study evaluates the efficacy and portability of the 29 airborne and synthetic satellite-based reflectance algorithms studied by Beck et al. (2016) for quantification of chlorophyll-a in two temperate reservoirs. It further extends the work of Augusto-Silva et al. (2014), as well, by using airborne hyperspectral imagery and dense coincident in-situ observations for a direct comparison between the performances of these algorithms across two lakes.

Augusto-Silva et al. (2014) reviewed the satellite reflectance algorithms, including two-band-algorithm (2BDA) (Dall'Olmo & Gitelson, 2005), three band-algorithm (3BDA) (Gitelson et al., 2003), and the Normalized Difference Chlorophyll Index (NDCI) algorithm (Mishra & Mishra, 2012), while Beck et al. (2016) added the Fluorescence Line Height algorithms (FLH) for the approximation of chlorophyll-a concentrations in inland lakes. The findings of these studies demonstrate the accuracy of sensor-based chlorophyll-a estimates (Sauer, Roesler, Werdell, & Barnard, 2012). Where accuracy was based on how close the imager-based proxy was to observed chloropyll-a concentration sampled directly from the water body and determined using a laboratory extraction method.

Due to differing band spacing and sensor configurations, it is important to note that not all algorithms can be applied to all sensors, and direct measurements of chlorophyll-a and phytoplankton communities in surface waters are highly variable due to nutrient, wind, and temperature fluxes, as well as a host of other bio-physical factors (Hunter, Tyler, Willby, & Gilvear, 2008; Sawaya et al., 2003; Stumpf et al., 2016; Wang, Xia, Fu, & Sheng, 2004). The comparison of multiple sensors is again complicated by the varying atmospheric and surface conditions that result from differing return times (Thonfeld, Feilhauer, & Menz, 2012). This issue is mitigated in this study by upscaling and spectral binning one hyperspectral image, the airborne-CASI. The advantage of this was we only needed to collect one set of coincident surface observations.

Another issue conflating the direct detection of HABs, which in freshwaters are most often caused by cyanobacteria, is that most current sensors lack the narrow band at 620nm corresponding to the phycocyanin absorption feature. Phycocyanin is more directly related to risk because it is a pigment produced by only cyanobacteria. Here the focus was solely on chlorophyll-a algorithms as proxies for any algal bloom. Given the current concern over HABs in general, and the evolving understanding of toxicity attributed algal communities, water safety professionals will likely want to acquire direct samples of any lake that the satellite imagery suggests is experiencing high chlorophyll-a concentrations.

In addition to assessing how the 29 algorithm-imager combinations perform between our study lakes, we also examined the site-specific variations that may impact imager performance for the following imagers: Compact Airborne Spectrographic Imager (CASI), WorldView-2, Sentinel-2, Landsat-8, MODIS, and MERIS. Finally, we apply an automated approach to image processing using the open source software, R, (R Core Team, 2017). This approach significantly decreases the time it takes to derive chlorophyll-a estimates so that multiple estimates may be considered simultaneously.

2. Methods

2.1. Study area

The study focuses on two temperate lakes roughly 150 kilometers apart: Taylorsville Lake in Central Kentucky and Harsha Lake (aka East Fork Lake) in Southwest Ohio. Taylorsville Lake has an approximate water surface area of 11.88 km², while Harsha's is 7.99 km² (Fig. 1). These lakes were chosen because they are both sites of recent and reoccurring algal blooms (including HABs), they share similar geography, and are subject to routine monitoring. Both lakes are sources of drinking water, support recreation areas containing beaches, host open water swimming, and are used for recreational fishing, so water safety concerns are high. Both lakes are reservoirs that were created in the late 1970's by the USACE for flood control.

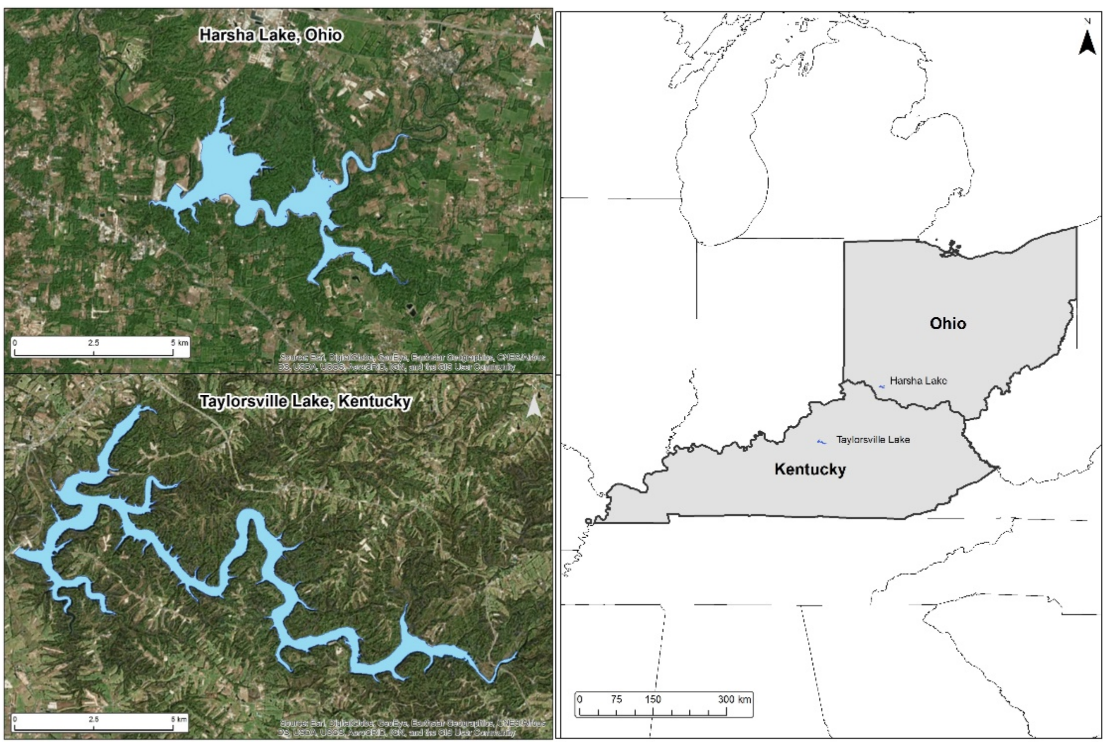

Fig 1. Map of the locations of the two studies, Harsha Lake near Cincinnati, Ohio and Taylorsville Lake in Central Kentucky.

2.2. Datasets

The datasets used in this research were the following: 1) Compact Airborne Spectrographic Imager (CASI) hyperspectral imagery (HSI), 2) coincident surface spectral observations collected using an Analytical Spectral Devices (ASD) brand spectroradiometer, and 3) in situ measurements made using in-vivo water sensors and analyzing surface water grab samples using laboratory and microscopy methods. These same datasets were used in Beck et al. (2016) for Harsha lake only. CASI-HSI was acquired via flyover for Taylorsville on 6/18/2014, while the Harsha flyover and sampling occurred on 6/27/2014. The USACE Joint Airborne Lidar Bathymetry Technical Center of Expertise (JALBTCX) supported the CASI-1500 airborne surveys while personnel from the USACE, USEPA, Kentucky Division of Water, and the University of Cincinnati all collaborated to acquire water quality and phytoplankton community measurements within one hour of the imagery acquisition.

2.3. Hyperspectral Imagery Acquisition

The acquisition of the CASI-1500 airborne HSI and radiometer collected images for Taylorsville lake on the morning of June 18, 2014. The system was flown at an altitude of approximately 2000 meters where it collected a 48-band hyperspectral image 1,466-meters wide at 1-meter spatial and 14-nanometer Full Width Half Maximum (FWHM) spectral resolution over a wavelength range of 371 to 1042 nm (Fig. 2). The detailed description of the hyperspectral image acquisition and pre-processing are available in Beck et al. (2016) section 2.4. Tests with extracted water pixel Fast Line-of-sight Atmospheric Analysis of Hypercubes (FLAASH) reflectance spectra after atmospheric correction were similar to spectral measurements made via boat with the ASD. Both display a strong peak at 714 nm associated with chlorophyll-a (Fig. 2).

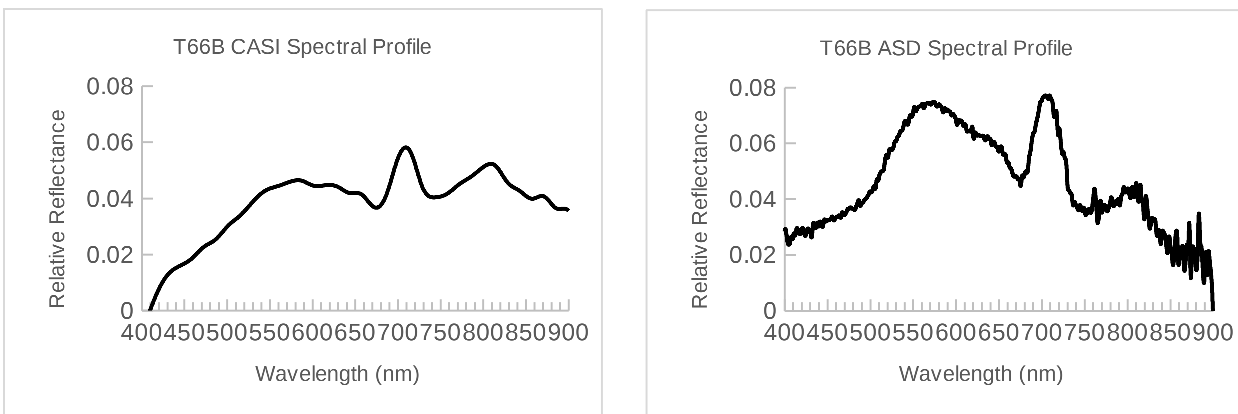

Fig. 2. Spectral profile of water at sample location T66B (Fig. 3) of Taylorsville Lake, KY, exhibiting a strong chlorophyll-a reflectance peak at 714 nanometers from atmospherically corrected CASI HSI data (left) and the same location measured at the water surface with a spectroradiometer in the field within one hour of the overflight (right). Y-axis is reflectance relative to calibration standards and the X-axis is scaled from 400 nm to 900 nm in both graphs.

2.4. Coincident surface observation procedures

The Taylorsville and Harsha Lake surface water sampling campaign was accomplished with four boats visiting 70 and 44 sites, respectively, to establish a 400-m grid point spacing. Surface observation collection was coordinated with the imaging aircraft via an air-to-ground radio. Each boat's crew collected the following:

1. Surface water grab samples from each sample point for subsequent laboratory measurements of general water quality constituents, algal pigments, and a subset of samples were processed for algae identification and enumeration.
2. ASD-brand spectroradiometer spectral signature to evaluate atmospheric correction of CASI imagery.
3. In situ sensor measurements using the YSI-brand chlorophyll, phycocyanin, turbidity, specific conductance, pH, water temperature, and dissolved oxygen sensor suite of a YSI 6600 data sonde (YSI Instruments, Yellow Springs, Ohio). The sondes were calibrated followed manufacturer guidelines and were cross-validated just prior to boat launch.
4. Secchi depth measurements.

5. GPS location- and date/time-referenced photos of surface water conditions at each sample point. All data were referenced to the WGS84 map datum and converted to the Universal Transverse Mercator (UTM) Zone 16 North map projection (Fig. 3).

Note, only the algal pigment and I&E information obtained from the grab samples are pertinent to the study goals here.

Grab samples were measured for chlorophyll-a by extraction and spectrophotometric detection according to Standard Method 10200H2.b (APHA et al., 2012). The summed values for pheophytin corrected chlorophyll-a and pheophytin (i.e., a so-called measure of uncorrected chlorophyll-a) and abbreviated here as SUMReCHL (μg/L)). This measure of total chlorophyll pigment more likely aligns with the reflectance of the in vivo chlorophyll pigments measured by the imagers. Algal I&E on a subset of samples (every other sample of each Lake's full sampling grid) was accomplished following the Standard Method membrane filtration technique (APHA et al., 2012).

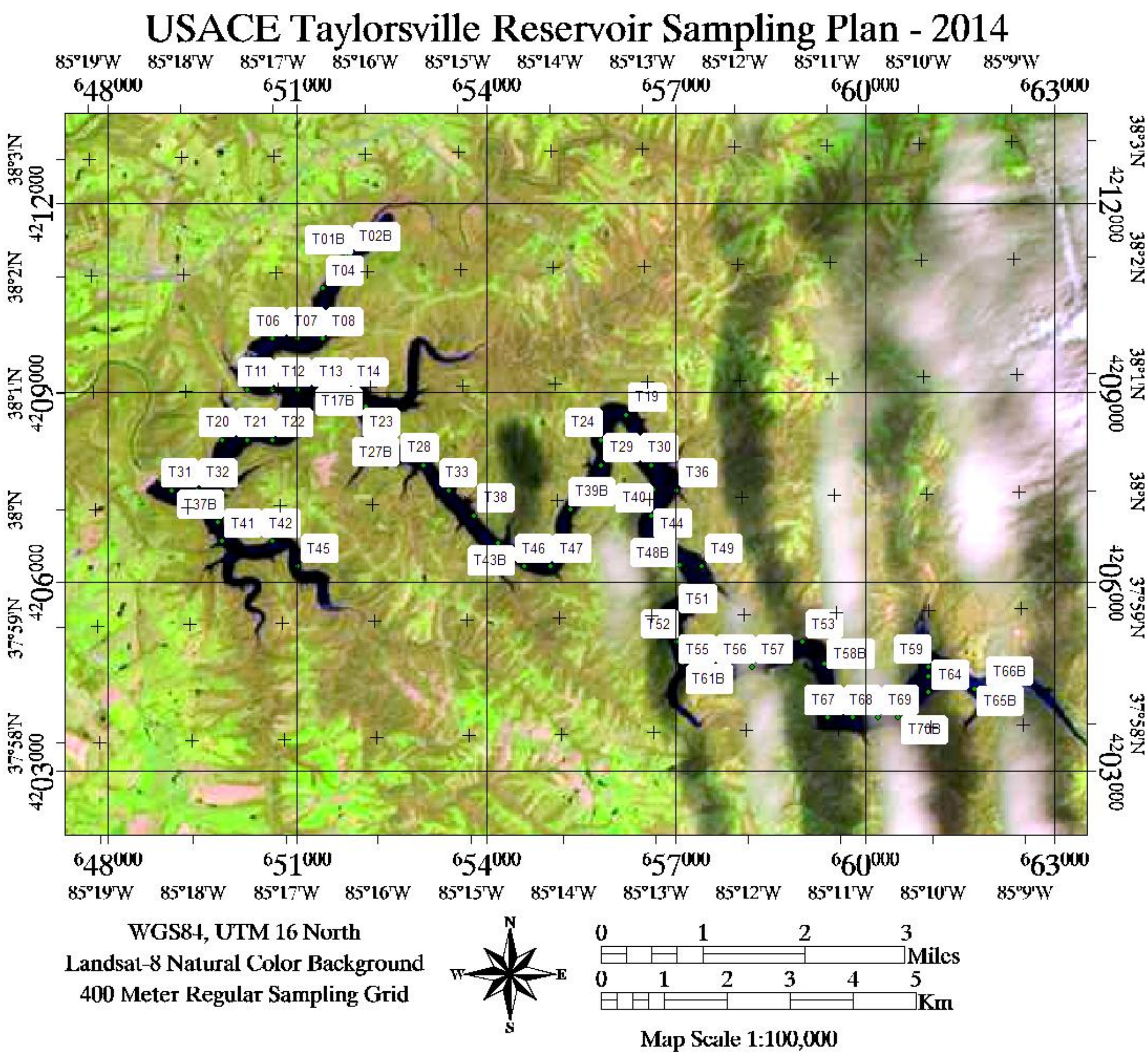

Fig. 3. Sampling scheme implemented on June 18th, 2014 for Taylorsville Lake to acquire water quality information from seventy sites within 1 h of image acquisition. (Source: United States Army Corps of Engineers).

2.5. Synthetic satellite imagery

The original airborne CASI HIS bands were spectrally averaged with equal weighting using band math in the *raster* package (Hijmans, 2016) for R to produce synthetic satellite image bands for Landsat-8, Sentinel-2, MERIS/OLCI, MODIS, and WorldView-2/3, according to published specifications (DigitalGlobe, 2009, 2014; ESA, 2012, 2013; USGS, 2015; Lindsey and Herring, 2001). Since the results from the spectral binning process are generated from the same original reflectance data set as well as the same series of dense coincident surface observations this approach eliminates the errors that arise from co-registration, atmospheric conditions, and surface fluxes that complicate the comparison of real imagery acquired at different times (Beck et al.,2016; Thonfeld et al., 2012). After spectral binning, these data were then spatially resampled to the appropriate resolution of each sensor (Table 1). This approach is not without uncertainty, the linear spectral resampling can introduce a root mean square error (RMSE) of 1 to 3% and 6 to 8% relative error, and similarly the spatial resampling process may produce 10-32% of relative error (Schlapfer et al. 1999; Schlapfer et al. 2002). Given the trade-offs associated with signal to noise ratio (SNR), sampling interval, and band configuration this research followed the recommendation set forth by Broge and Mortensen (2002) to spectrally and spatially resample hyperspectral imagery to mimic coarser sensors. This approach has been successfully applied to OLCI by Augusto-Silva et al. (2014), MERIS by Koponen et al. (2002), and expanded to include additional sensor configurations in Beck et al. (2016).

Sensor spatial resolution and lake geometry must be considered because the acquisition of water only pixels is critical for evaluating the algorithm performance via regression analysis. A minimum of three pure water pixels are required to perform a linear regression, but at least ten points are recommended for a more robust analysis (Picard and Cook, 1984; Stone, 1974). For a full description of this methodology see Beck et al. (2016) section 2.6. A deviation from the original study is the transition from Environment for Visualizing Images (ENVI) software to R , which allowed for automation of all aspects of this research. This is also a step toward operational remote sensing systems, and for the complete R script see Johansen (2017). To ensure there were no differences between the methods, pixel values from both studies were evaluated at multiple randomly chosen points for each of the chlorophyll-a algorithms. All of the pixels evaluated displayed the same values regardless of which software was chosen to do the computation, so no further modifications were needed to transfer the methods from the original ENVI formats to the R scripts used in this study (data not shown). Table 1 displays the band combinations of the original sensors as well as modified synthetic configurations. The objective was to recreate the original sensors using the CASI band configurations to keep the synthetic band widths and centers as close as possible.

Table 1
Original CASI and synthetic sensor band configurations

IMAGER	ORIGINAL RANGE (NM)	CENTER (NM)	BANDWIDTH (NM)	SYNTHETIC RANGE (NM)	SYNTHETIC CENTER (NM)	BAND WIDTH (NM)
WORLDVIEW-2/3				Resampled to 1.8 m		
B1	400–450	425	50	400.3–444.4	428.9	44
B2	450–510	480	60	457.8–515.1	486.5	57
B3	510–580	545	70	515.1–586.5	550.8	71
B4	585–625	605	40	586.5–629.3	607.9	43
B5	630–690	660	60	629.3–686.2	657.75	57
B6	705–745	725	40	700.4–743.1	721.75	43
B7	770–895	832.5	125	771.5–899.7	835.6	128

B8	860–1040	950	180	856.9–1042.7	949.8	186
SENTINEL-2				Resampled to 20 m		
B1	433-453	443	20	429.0–457.8	443.4	29
B2	458–523	490.5	65	457.8–529.4	493.4	72
B3	543–578	560.5	35	543.7–572.2	557.9	29
B4	650–680	665	30	643.5–686.2	664.8	43
B5	698–713	705.5	15	700.4–714.6	707.5	14
B6	733–748	740.5	15	728.9–757.3	743.1	28
B7	773–793	783	20	771.5–800.0	785.7	29
B8	785–900	842.5	115	785.8–899.7	842.7	114
B8B	855–875	865	20	856.9–885.4	864.0	26
B9	935–955	945	20	928.2–956.8	942.5	29
LANDSAT-8				Resampled to 30 m		
B1	430–450	440	20	429.0–457.8	443.4	28
B2	450–510	480	60	457.8–500.8	479.3	43
B3	530–590	560	60	529.4–586.5	557.9	57
B4	640–670	655	30	643.5–672.0	657.7	29
B5	850–880	865	30	842.7–885.4	864.0	43
MERIS/OLCI				Resampled to 300 m		
B1	402–412	407	10	400.3–414.7	407.5	14
B2	438–448	443	10	429.0–457.8	443.4	29
B3	485–495	490	10	486.5–500.8	493.6	14
B4	505–515	510	10	500.8–515.1	507.9	14
B5	555–565	560	10	558.0–572.2	565.1	14
B6	615–625	620	10	615.0–629.3	622.1	14
B7	660–670	665	10	657.7–672.0	664.8	14
B8	678–685	681.5	7	672.0–686.2	679.1	14
B9	704–714	709	10	700.4–714.6	707.5	14
B10	750–757	753.5	7	743.1–757.3	750.2	14
B11	757–762	759.5	5	757.3–771.5	764.4	14
B12	772–787	779.5	15	771.5–785.8	778.5	14
B13	855–875	865	20	856.9–871.2	864.0	14
B14	880–890	885	10	871.2–899.7	885.4	29
B15	895–905	900	10	885.4–913.9	899.6	29
MODIS				Resampled to 250 m		
B1	620–670	645	50	615.0–672.0	643.5	57
B2	841–876	858.5	35	842.7–871.2	856.9	29

2.6. Image analysis

This methodology was utilized by forth by Beck et al. (2016) who further extended the work of Augusto-Silva et al. (2014) in which airborne hyperspectral imagery was used in the place of surface measurements collected via spectroradiometer (Mittenzwey, Ulrich, Gitelson, & Kondratiev, 1992; Kallio, 2000; Koponen et al., 2002). The advantages of deriving the synthetic satellite imager versions are detailed by Reif (2011). This research applied all of the algorithms used in Augusto-Silva et al. (2014) and the more recent set of hybrid algorithms developed my Beck et al. (2016), which include the following: Cyanobacterial Index (CI), Maximum Chlorophyll Index (MCI), series of Fluorescence Line Height (FLH/FLH Blue/FLH Violet), and Surface Algal Bloom Index (SABI) algorithms, two band-algorithms (2BDA), three band-algorithm (3BDA), and 3BDA-like (KIVU) (Alawadi, 2010; Beck et al., 2016; Binding et al., 2013; Brivio et al., 2001; Chipman, Olmanson, & Gitelson, 2009; Dall'Olmo & Gitelson, 2005; Gitelson et al., 2003; Mishra & Mishra, 2012; Wynne et al., 2012; Zhao et al., 2010;). Table 2 contains the full list of chlorophyll-a algorithms, their abbreviations, and the band math for each algorithm evaluated.

Table 2

Band math and wavelengths in nm for each algorithm used for chlorophyll-a estimation at Harsha Lake. Float refers to floating point values.

Chlorophyll-a index algorithms by satellite/sensor	Spatial res. (m)	Band math/wavelengths (nm)
CASI CI	1	-1*((CASI[[23]])-(CASI[[22]]-(CASI[[25]]-CASI[[22]])))
CASI CI	1	-1*(((float(686))-(float(672))-((float(714))-(float(672)))))
CASI MCI	1	((CASI[[23]])-(CASI[[22]]-(CASI[[25]]-CASI[[22]])))
CASI MCI	1	(((float(686))-(float(672))-((float(714))-(float(672)))))
CASI FLH	1	(CASI[[25]]-(CASI[[27]]+(CASI[[23]]-CASI[[27]])))
CASI FLH	1	(float(714))-[float(743) + (float(686)-float(743))]
CASI NDCI	1	(CASI[[25]]-CASI[[23]])/(CASI[[25]]+CASI[[23]])
CASI NDCI	1	(float(714)-float(686))/(float(714) + float(686))
CASI 2BDA	1	(CASI[[25]])/(CASI[[22]])
CASI 2BDA	1	(float(714))/(float(672))
CASI 3BDA	1	((1/CASI[[22]])-(1/CASI[[25]]))*(CASI[[28]])
CASI 3BDA	1	((1/float(672))-(1/float(714)))*(float(757))
WorldView-2 and -3 NDCI	1.8	(WV2[[6]]-WV2[[5]])/(WV2[[6]]+WV2[[5]])
WorldView-2 and -3 NDCI	1.8	(float(722)-float(658))/(float(722) + float(658))
WorldView-2 and -3 FLH violet	1.8	(WV2[[3]])-(WV2[[5]]+(WV2[[1]]-WV2[[5]]))
WorldView-2 and -3 FLH violet	1.8	((float(551))-[float(658) + (float(429)-float(658))])
WorldView-2 2BDA	1.8	(WV2[[6]])/(WV2[[5]])
WorldView-2 2BDA	1.8	(float(722))/(float(658))
WorldView-2 3BDA	1.8	((1/WV2[[5]])-(1/WV2[[6]]))*(WV2[[7]])
WorldView-2 3BDA	1.8	((1/float(658))-(1/float(722)))*(float(836))
Sentinel-2 NDCI	20	(S2[[5]]-S2[[4]])/(S2[[5]]+S2[[4]])
Sentinel-2 NDCI	20	(float(708)-float(665))/(float(708) + float(665))
Sentinel-2 FLH violet	20	(S2[[3]])-(S2[[4]]+(S2[[2]]-S2[[4]]))
Sentinel-2 FLH violet	20	((float(558))-[float(665) + (float(493)-float(665))])
Sentinel-2 2BDA	20	(S2[[5]])/(S2[[4]])
Sentinel-2 2BDA	20	(float(708))/(float(665))
Sentinel-2 3BDA	20	((1/S2[[4]])-(1/S2[[5]]))*(S2[[9]])
Sentinel-2 3BDA	20	((1/float(665))-(1/float(708)))*(float(864))
*Landsat-8 NIR band is far from chlorophyll-a peak Landsat-8 NDCI	30	(L8[[5]]-L8[[4]])/(L8[[5]]+L8[[4]])
Landsat-8 NDCI	30	(float(864)-float(658))/(float(864) + float(658))
Landsat-8 SABI	30	(L8[[5]]-L8[[4]])/(L8[[2]]+L8[[3]])
Landsat-8 SABI	30	(float(864)-float(658))/(float(479) + float(558))
Landsat-8 FLH blue	30	(L8[[3]])-(L8[[4]]+(L8[[2]]-L8[[4]]))
Landsat-8 FLH blue	30	(float(558))-[float(657) + (float(480)-float(658))]
Landsat-8 FLH violet	30	(L8[[3]])-(L8[[4]]+(L8[[1]]-L8[[4]]))
Landsat-8 FLH violet	30	(float(558))-[float(658) + (float(443)-float(658))]
Landsat-8 2BDA	30	(L8[[5]])/(L8[[4]])
Landsat-8 2BDA	30	(float(864))/(float(658))
Landsat-8 KIVU (3BDA-like)	30	(L8[[2]]-L8[[4]])/(L8[[3]])
Landsat-8 KIVU (3BDA-like)	30	(float(479)-float(658))/(float(558))
Landsat-8 3BDA	30	((1/L8[[2]])-(1/L8[[4]]))*(L8[[3]])
Landsat-8 3BDA	30	((1/float(479))-(1/float(658)))*(float(558))
MODIS NDCI	250	(MODIS[[2]]-MODIS[[1]])/(MODIS[[2]]+MODIS[[1]])
MODIS NDCI	250	(float(857)-float(644))/(float(857) + float(644))
MODIS 2BDA	250	(MODIS[[2]])/(MODIS[[1]])
MODIS 2BDA	250	(float(857))/(float(644))
MERIS CI	300	(-1*((MERIS[[8]])-(MERIS[[7]])-((MERIS[[9]])-(MERIS[[7]]))))
MERIS CI	300	-1*(((float(679))-(float(665))-((float(708))-(float(665)))))
MERIS MCI	300	((MERIS[[9]])-(MERIS[[8]])-((MERIS[[10]])-(MERIS[[8]])))
MERIS MCI	300	(((float(708))-(float(679))-((float(750))-(float(679)))))
MERIS FLH	300	(MERIS[[9]])-(MERIS[[10]]+(MERIS[[8]]-MERIS[[10]]))
MERIS FLH	300	(float(708))-[float(750) + (float(679)-float(750))]
MERIS NDCI	300	(MERIS[[9]]-MERIS[[7]])/(MERIS[[9]]+MERIS[[7]])

MERIS NDCI	300	(float(708)-float(665))/(float(708) + float(665))
MERIS 2BDA	300	(MERIS[[9]])/(MERIS[[7]])
MERIS 2BDA	300	(float(708))/(float(665))
MERIS 3BDA	300	((1/MERIS[[7]])-(1/MERIS[[9]]))*(MERIS[[11]])
MERIS 3BDA	300	((1/float(665))-(1/float(708)))*(float(764))

2.7 Algorithm Evaluation and Model Validation

The standard Type-1 regression test (Pinero, Perelman, Guerschman, & Paruleo, 2008; Kudela et al., 2015; Beck et al., 2016) was used for the newly reported 70 laboratory observations of chlorophyll-a (SumReChl (µg/L)) that corresponded to the cloud-free pixels for each of the following sensors: CASI, synthetic WorldView-2, synthetic Sentinel-2, synthetic Landsat-8, synthetic MODIS, and synthetic MERIS. Each pair of pixels and surface observations were compared and evaluated using the Pearson's r^2 correlation and are shown in Table 3 and 4 under the global algorithm heading corresponding to the simple linear model's p-value, slope, and intercept.

For comparison and model validation a robust repeated k-folds cross-validation method was applied for all the data sets (Picard and Cook, 1984; Stone, 1974). The method used three folds which divide the measurements into random groupings, and then subsequently uses two groups (2/3 of the samples) for model calibration and the remaining group (1/3 of samples) for validation. This process is done so that each combination of 2/3 to 1/3 is applied. This process is then iterated through five times, and in each iteration the groups are populated with randomly assigned samples. The repeated k-folds method produces average r^2, root mean square error (RMSE), r^2, and mean average error (MAE) derived from all fifteen models for each of the 29 algorithms. This robust cross-validation method is done for each sensor-algorithm pair for each lake shown in Table 3 and 4 under the cross-validated average heading. These data are then normalized to calculated chlorophyll-a values for all of the algorithms from the Type-1 regression tests, which allows for a fair comparison of the performance of each of the indices (Beck et al., 2016; Kudela et al., 2015). To accommodate that certain researchers prefer the use of the Type-2 geometric mean method, designed to test correlations in natural systems (Peltzer, 2015) we applied this to the chlorophyll-a estimations at Taylorsville Lake (Table 6).

3. Results

Each image derived chlorophyll-a index had a single-band output calculated (Table 2) that was compared with the coincident surface observations of chlorophyll-a at both Taylorsville Lake and Harsha Lake. To evaluate the performance of each algorithm standard Type-1 regression test (Pearson's r), of the chlorophyll-a algorithms derived from the atmospherically corrected imagery following Pinero et al. (2008) and Kudela et al. (2015) with a p-value threshold of 0.001 was undertaken, the result of which are in Table 3 and 4 corresponding to Taylorsville and Harsha Lake, respectively. Pixels that were not pure water pixels were excluded to mitigate the algorithm from conflating land vegetation with aquatic vegetation or algae.

Table 3

Performance of algorithms for chlorophyll-a estimation at Taylorsville Lake using chlorophyll-a indices according to Pearson's r test (Type-1) linear regressions and k-folds cross-validation.

		Global Algorithm				Cross-Validated Average		
Algorithms	**No. of Points**	**r^2**	**p-value**	**Slope**	**Intercept**	**r^2**	**RMSE**	**MAE**
CASI CI	70	0.678	<0.001	0.642	21.677	0.689	16.345	12.238
CASI MCI	70	0.481	<0.001	0.539	21.745	0.511	20.210	15.300

CASI FLH	70	0.678	<0.001	0.642	21.677	0.683	16.016	12.126
CASI NDCI	70	0.575	<0.001	401.211	21.34	0.597	18.281	14.473
CASI 2BDA	70	0.658	<0.001	146.489	-131.003	0.668	16.792	13.007
CASI 3BDA	70	0.604	<0.001	169.812	15.953	0.641	18.122	14.034
WV2 NDCI	70	0.488	<0.001	504.827	32.776	0.507	20.318	15.521
WV2 FLH violet	70	0.188	<0.001	0.558	-86.486	0.216	25.310	19.609
WV2 2BDA	70	0.499	<0.001	244.43	-212.303	0.511	19.946	15.217
WV2 3BDA	70	0.442	<0.001	225.43	32.479	0.491	21.360	15.527
S2 NDCI	69	0.698	<0.001	554.162	7.204	0.713	15.507	11.840
S2 FLH violet	69	0.228	<0.001	1.489	30.85	0.252	24.206	18.878
S2 2BDA	69	0.707	<0.001	239.526	-230.765	0.724	16.304	12.181
S2 3BDA	69	0.588	<0.001	256.55	9.001	0.616	18.248	13.184
L8 NDCI	69	0.012	0.375	-53.498	39.285	0.053	28.042	21.798
L8 SABI	69	0.017	0.288	-44.96	39.789	0.042	27.641	21.404
L8 FLH blue	69	0.317	<0.001	0.972	-23.625	0.319	23.019	18.088
L8 FLH violet	69	0.308	<0.001	0.696	-51.341	0.322	23.499	18.332
L8 2BDA	69	0.009	0.437	-21.212	60.267	0.030	27.555	21.552
L8 KIVU	69	0.099	0.008	80.752	71.521	0.124	26.310	18.935
L8 3BDA	69	0.119	0.004	-74.272	78.442	0.136	26.021	18.633
MODIS NDCI	10	0.008	0.804	-34.494	28.393	0.317	18.054	14.568
MODIS 2BDA	10	0.012	0.758	-20.866	49.409	0.412	17.189	14.122
MERIS*	3	N/A	N/A	N/A	N/A	N/A	N/A	N/A

* The MERIS configuration only produced three usable water only pixels, which did not meet the minimal requirements to derive Pearson's r statistical correlations.

Table 4

Performance of algorithms for chlorophyll-a estimation at Harsha Lake using chlorophyll-a indices according to Pearson's r test (Type-1) linear regressions and k-folds cross-validation.

		Global Algorithm				**Cross-Validated Average**		
Algorithms	**No. of Points**	**R^2**	**p-value**	**Slope**	**Intercept**	**R^2**	**RMSE**	**MAE**
CASI CI	42	0.688	<0.001	0.183	35.288	0.691	9.076	7.335
CASI MCI	42	0.528	<0.001	0.210	15.606	0.569	11.414	8.641
CASI FLH	42	0.688	<0.001	0.183	35.288	0.683	9.063	7.333
CASI NDCI	42	0.673	<0.001	166.715	33.399	0.689	9.387	7.454
CASI 2BDA	42	0.712	<0.001	61.174	-25.556	0.725	8.884	6.871
CASI 3BDA	42	0.706	<0.001	107.462	35.626	0.710	8.905	6.835
WV2 NDCI	42	0.711	<0.001	193.646	56.438	0.718	8.731	6.605
WV2 FLH	42	0.449	<0.001	0.492	-95.533	0.492	12.105	9.319

violet								
WV2 2BDA	42	0.712	<0.001	97.963	-42.507	0.712	8.612	6.564
WV2 3BDA	42	0.697	<0.001	144.901	55.555	0.699	8.990	6.607
S2 NDCI	41	0.700	<0.001	212.912	34.847	0.737	8.838	6.491
S2 FLH violet	41	0.030	0.282	-0.294	59.466	0.098	16.679	14.423
S2 2BDA	41	0.711	<0.001	88.635	-53.107	0.707	8.876	6.587
S2 3BDA	41	0.679	<0.001	175.218	36.026	0.679	9.022	7.059
L8 NDCI	41	0.108	0.036	55.402	65.590	0.165	15.505	13.337
L8 SABI	41	0.097	0.048	75.738	68.393	0.125	15.859	13.427
L8 FLH blue	41	0.106	0.038	0.410	6.513	0.162	15.534	12.560
L8 FLH violet	41	0.355	<0.001	0.479	-46.818	0.375	13.319	10.630
L8 2BDA	41	0.106	0.038	44.651	24.576	0.157	15.592	13.219
L8 KIVU	41	0.029	0.289	-116.670	21.434	0.112	17.005	14.505
L8 3BDA	41	0.006	0.636	36.975	37.210	0.075	16.803	14.236
MODIS NDCI	19	0.187	0.065	45.124	62.745	0.323	11.556	9.555
MODIS 2BDA	19	0.202	0.054	40.650	26.924	0.259	9.541	7.844
MERIS CI	14	0.847	<0.001	0.210	31.302	0.877	3.757	3.249
MERIS MCI	14	0.178	0.133	0.099	28.420	0.491	11.316	8.593
MERIS FLH	14	0.847	<0.001	0.210	31.302	0.865	3.848	3.434
MERIS NDCI	14	0.847	<0.001	201.561	35.514	0.842	4.175	3.612
MERIS 2BDA	14	0.848	<0.001	87.944	-51.956	0.901	4.408	3.895
MERIS 3BDA	14	0.845	<0.001	152.148	36.792	0.870	4.077	3.279

Table 5

Normalized performance of algorithms for chlorophyll-a estimation at Taylorsville and Harsha Lake using chlorophyll-a indices according to Pearson's r test (Type-1) linear regressions. This test is used to normalize the slope and intercepts to facilitate a direct comparison between algorithms following the method of Kuedela et al. (2015).

	Taylorsville			**Harsha**		
Algorithms	r²	Slope	Intercept	r²	Slope	Intercept
CASI CI_Chla	0.678	1.000	0.004	0.688	1.002	-0.085
CASI MCI_Chla	0.481	1.001	-0.017	0.528	1.001	-0.011
CASI FLH_Chla	0.678	1.000	0.004	0.688	1.002	-0.085
CASI NDCI_Chla	0.575	1.000	0.000	0.673	1.000	0.000
CASI 2BDA_Chla	0.658	1.000	0.000	0.712	1.000	0.000
CASI 3BDA_Chla	0.604	1.000	0.000	0.706	1.000	0.000
WV2 NDCI_Chla	0.488	1.000	0.000	0.711	1.000	0.000
WV2 FLH violet_Chla	0.188	1.000	0.009	0.449	1.000	-0.008
WV2 2BDA_Chla	0.499	1.000	0.001	0.712	1.000	0.000
WV2 3BDA_Chla	0.442	1.000	0.000	0.697	1.000	0.000

S2 NDCI_Chla	0.698	1.000	0.000	0.700	1.000	0.000
S2 FLH violet_Chla	0.228	1.000	0.009	0.030	1.001	-0.065
S2 2BDA_Chla	0.707	1.000	0.001	0.711	1.000	0.000
S2 3BDA_Chla	0.588	1.000	0.000	0.679	1.000	0.000
L8 2NDCI_Chla	0.012	1.000	0.000	0.108	1.000	-0.001
L8 SABI_Chla	0.017	1.000	0.000	0.097	1.000	0.001
L8 FLH blue_Chla	0.317	1.000	-0.009	0.106	0.999	0.006
L8 FLH violet_Chla	0.308	1.000	0.012	0.355	1.000	-0.022
L8 2BDA_Chla	0.009	1.000	-0.001	0.106	1.000	-0.001
L8 KIVU_Chla	0.099	1.000	-0.001	0.029	1.000	0.000
L8 3BDA_Chla	0.119	1.000	0.000	0.006	1.000	0.000
MODIS NDCI_Chla	0.008	1.000	0.000	0.187	1.000	-0.001
MODIS 2BDA_Chla	0.013	1.000	-0.002	0.202	1.000	0.001
MERISWy08CI	N/A	N/A	N/A	0.847	1.000	0.002
MERISGo04MCI	N/A	N/A	N/A	0.178	1.000	-0.005
MERISZh10FLH	N/A	N/A	N/A	0.847	1.000	0.002
MERISMM12NDCI	N/A	N/A	N/A	0.847	1.000	0.000
MERISBe162BDA	N/A	N/A	N/A	0.848	1.000	0.000
MERISBe163BDA	N/A	N/A	N/A	0.845	1.000	0.000

3.1 Real Aircraft and Synthetic Satellite Imagery Results

CASI Imagery (Real):

Six algorithms (CI, MCI, FLH, NDCI, 2BDA and 3BDA) were evaluated using the atmospherically corrected CASI-1500 hyperspectral imagery. All six algorithms performed strongly and are ranked in order of highest to lowest Pearson's r^2 value, CASI CI, CASI FLH, CASI 2BDA, CASI 3BDA, CASI NDCI, and CASI MCI. Fig. 4 shows an imager-estimated chlorophyll-a map for Taylorsville lake using the top performing CASI-WY08CI algorithm. The high r^2 values are expected given the band configurations of the CASI HSI and the well-placed bands of 700 nm and 714 nm that highly correlate with spectral signatures of chlorophyll-a (Gitelson, 1992; Zhao et al., 2010). Although there is a change in the ranking of the sane algorithms between the lakes, all cross-validated models performed well at both lakes with ranges of r^2 values ranges of 0.569-0.725 at Harsha Lake and 0.511-0.689 at Taylorsville Lake. The RMSE ranged from 8.731-11.414 at Harsha Lake and 16.345 – 20.21 at Taylorsville Lake. The highest performing algorithms were CI and 2BDA.

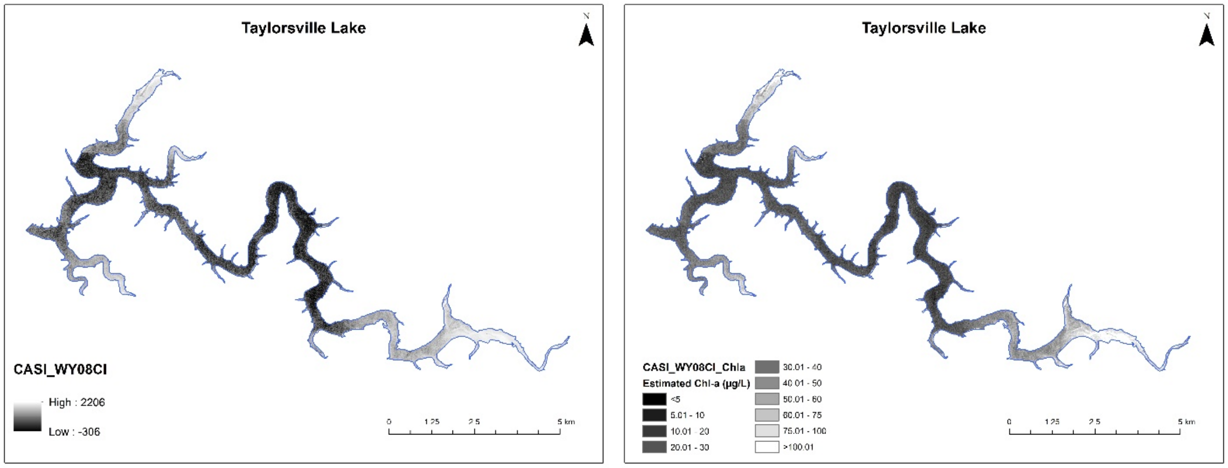

Fig. 4. **A** Results of the best performing CASI algorithm, CASI_Wy08CI, as the algorithm index values as applied to original CASI HSI imagery (shoreline in Blue) with brighter pixels indicating higher chlorophyll-a concentrations. Pearson's $r^2 = 0.678$, p-value <0.001, N = 70. **B** Estimated cholorphyll-a content (µg/L) by applying the slope and intercept from table 3 (0.642x + 21.667) to the raw CASI_Wy08CI algorithm values.

WorldView-2 (Synthetic):

This study evaluated four WorldView-2 algorithms (NDCI, FLH Violet, 2BDA and 3BDA) using the synthetically created WorldView-2 dataset. There was a noticeable decline in the performance of WorldView-2 algorithms in Taylorsville Lake with average r^2 values ranging from 0.216-0.511, and RMSEs from 19.946-25.31. WorldView-2 algorithm performance at Harsha was higher with average r^2 values ranging from 0.492-0.718, and RMSEs from 8.612-12.105. Even with the decline in performance, the NDCI and 2BDA algorithms were comparable with r^2 values over 0.5 for both lakes. The FLH-Violet algorithm performed poorly for both lakes, this result was not surprising since the algorithm was designed specifically for the broad bands of Landsat-8.

Sentinel-2 (Synthetic):

The same four algorithms were again tested using the synthetically created Sentinel-2 image. Three of these algorithms (NDCI, 2BDA, and 3BDA) demonstrated portability with r^2 values greater than 0.6 for both lakes. The Sentinel-2 derived NDCI and 2BDA algorithms exhibited very high comparable, with r^2 values greater than 0.7 for both lakes. The RMSE values for these two algorithms are 15.507-16.305 for Taylorsville and 8.838-8.876 at Harsha. All the Sentinel-2 algorithms are considered portable except the FLH-Violet, which was designed for Landsat-8. Sentinel-2 algorithms suggest more portability than even the original CASI derived algorithms, suggesting the spatial and spectral configurations of Sentinel-2 would as appropriate for detecting algal blooms without expensive flyover logistics.

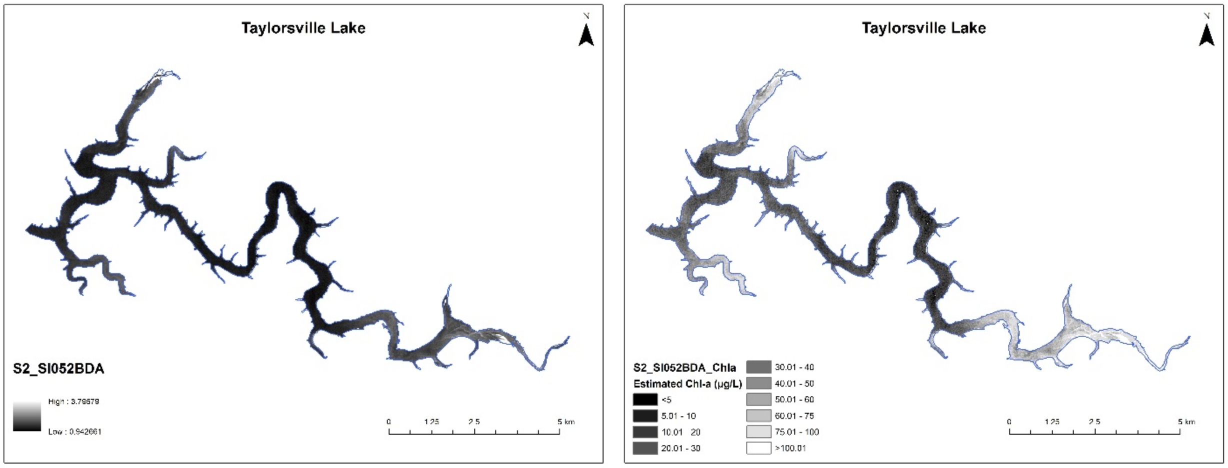

Fig. 5. **A** Results of the best performing Sentinel-2 algorithm, S2_SI052BDA, as algorithm index values as applied to synthetic Sentinel-2 imagery (shoreline in Blue) with brighter pixels in the indicating higher chlorophyll-a concentrations. Pearson's $r^2 = 0.707$, p-value <0.001, N = 69 (to avoid shoreline). **B** Estimated chlorophyll-a content (µg/L) by applying the slope and intercept from table 3 (239.526x – 230.765) to the raw S2_SI052BDA algorithm values.

Landsat-8 (Synthetic):

Seven algorithms (NDCI, SABI, FLH Blue, FLH Violet, 2BDA, KIVU, and 3BDA) were tested using the synthetically created Landsat-8 image, but all produced relatively poor results with a slight exception of the FLH algorithms. The band configuration of Landsat-8 affects its ability to detect the peak wavelength of chlorophyll-a, and subsequently diminishes the applicability and transferability of these algorithms. The newly developed FLH Blue and Violet algorithms captured some of the visible green peak and overcome these limitations with low to moderate success (Beck et al., 2016). Even with the enhanced FLH-Violet algorithm the r^2 values peak at 0.322 and 0.375 for Taylorsville and Harsha respectively. This suggested not only are Landsat-8 algorithms not portable, but extreme caution should be used if these algorithms are utilized on any similar-sized lake.

MODIS (Synthetic)

Only two chlorophyll-a algorithms were evaluated due to the spectral configurations of the MODIS sensor. The algorithms performed poorly with r^2 values ranging from 0.317-0.412 at Taylorsville and 0.259-0.323 at Harsha Lake, suggesting these are not well suited for algal bloom detection and are not portable across lakes. Another issue with MODIS is the spatial resolution of 250-meter pixels, which allowed for acquisition and subsequent analysis of 10 water-only pixels at Taylorsville Lake and 19 water-only pixels at Harsha. Given the low number of pixels, which tend to cluster in the large open areas of both lakes, makes capturing the variation of chlorophyll-a concentration within a lake difficult. This lack of variation coupled with MODIS's spectral and spatial configurations limits the use of this sensor for small to midsized lakes.

MERIS (Synthetic)

MERIS has been well studied for the detection of algal blooms in water bodies, especially large lakes and marine environments. This study evaluated six chlorophyll-a algorithms (CI, MCI, FLH, NDCI, 2BDA and 3BDA) and ran into the same concerns of spatial resolution at Taylorsville with only three usable pixels (T32, T54, and T59). This was deemed insufficient to accurately measure any statistical correlation or portability. However, the performance of the MERIS algorithms at Harsha Lake with 14 usable pixels, suggests MERIS is well suited for algal bloom detection in appropriately sized systems. Five of the six algorithms performed extremely well with r^2 ranges of 0.865-0.901 and RMSEs of only 3.757-4.408. The MCI algorithm had a low-moderate performance with r^2 of 0.491 and RMSE of 11.316. Further examination is needed to compare the portability of MERIS given its very high performance at Harsha Lake. Unfortunately, the 300-meter spatial resolution of MERIS is a major limiting factor in the acquisition of water-only pixels in narrow width, lakes, such as Taylorsville, which is a common feature of many run-of-the-river derived reservoirs.

Table 6

Performance of algorithms for chlorophyll-a estimation at Taylorsville Lake and Harsha Lake using chlorophyll-a indices according to Peltzer (2015) Type 2 Geometric Mean Tests. Included for completeness because type-2 Geometric Mean Test is designed to evaluate the correlations values in natural systems, which some researchers prefer over the Type-1 method above.

	Taylorsville					Harsha				
Algorithms	**r^2**	**Slope**	**Intercept**	**STD Slope**	**STD Intercept**	**r^2**	**Slope**	**Intercept**	**STD Slope**	**STD Intercept**
CASI CI	0.678	1.214	-7.88	0.087	3.779	0.688	1.208	-10.572	0.111	5.868
CASI MCI	0.481	1.443	-16.268	0.137	5.671	0.528	1.377	-19.179	0.161	8.409
CASI FLH	0.678	1.214	-7.88	0.087	3.779	0.688	1.208	-10.572	0.111	5.868
CASI NDCI	0.575	1.318	-11.705	0.111	4.697	0.673	1.219	-11.176	0.116	6.084
CASI 2BDA	0.658	1.233	-8.563	0.092	3.952	0.712	1.185	-9.454	0.105	5.527
CASI 3BDA	0.604	1.287	-10.54	0.104	4.429	0.706	1.190	-9.702	0.106	5.609
WV2 NDCI	0.488	1.431	-15.862	0.135	5.591	0.711	1.186	-9.473	0.105	5.534
WV2 FLH violet	0.188	2.305	-47.983	0.298	11.499	0.449	1.493	-25.158	0.192	9.997
WV2 2BDA	0.499	1.416	-15.307	0.132	5.476	0.712	1.186	-9.465	0.105	5.531
WV2 3BDA	0.442	1.504	-18.544	0.149	6.134	0.697	1.198	-10.104	0.109	5.741
S2 NDCI	0.698	1.197	-7.294	0.084	3.66	0.700	1.195	-9.934	0.109	5.753
S2 FLH violet	0.228	2.093	-40.511	0.261	10.281	0.030	5.818	-244.893	1.199	61.022
S2 2BDA	0.707	1.189	-7	0.082	3.58	0.711	1.186	-9.435	0.106	5.586
S2 3BDA	0.588	1.305	-11.291	0.109	4.648	0.679	1.214	-10.875	0.115	6.060
L8 NDCI	0.012	9.218	-304.591	1.504	55.917	0.108	3.041	-103.719	0.564	28.823
L8 SABI	0.017	7.715	-248.877	1.244	46.304	0.097	3.215	-112.547	0.604	30.854
L8 FLH blue	0.317	1.775	-28.757	0.203	8.149	0.106	3.073	-105.472	0.572	29.228
L8 FLH violet	0.308	1.802	-29.682	0.208	8.323	0.355	1.679	-34.560	0.242	12.511
L8 2BDA	0.009	10.522	-352.947	1.729	64.262	0.106	3.074	-105.405	0.572	29.212
L8 KIVU	0.099	3.171	-80.469	0.453	17.259	0.029	5.898	-248.915	1.217	61.944
L8 3BDA	0.119	2.896	-70.273	0.405	15.493	0.006	13.146	-617.259	2.861	145.464
MODIS NDCI	0.008	11.072	-283.231	5.28	148.712	0.187	2.315	-65.068	0.598	29.740
MODIS 2BDA	0.013	8.938	-223.237	4.212	118.725	0.202	2.225	-60.629	0.566	28.156
MERIS CI	N/A	N/A	N/A	N/A	N/A	0.847	1.087	-4.089	0.125	6.014
MERIS MCI	N/A	N/A	N/A	N/A	N/A	0.178	2.371	-64.798	0.736	34.907
MERIS FLH	N/A	N/A	N/A	N/A	N/A	0.847	1.087	-4.089	0.125	6.014
MERIS NDCI	N/A	N/A	N/A	N/A	N/A	0.847	1.087	-4.101	0.125	6.023
MERIS 2BDA	N/A	N/A	N/A	N/A	N/A	0.848	1.086	-4.048	0.124	5.980

MERIS 3BDA	N/A	N/A	N/A	N/A	N/A	0.845	1.088	-4.145	0.126	6.057

4. Discussion

This research utilized atmospherically corrected airborne CASI hyperspectral imagery to develop synthetic WorldView-2, Sentinel-2, Landsat-8, MODIS, and MERIS imagery coupled with dense coincident water surface observations to evaluate the performance and portability of twenty-nine chlorophyll-a algorithms for two temperate inland lakes. The results demonstrate a high-level of confidence in the portability of certain algorithm-sensor pairs proposed in this study. Furthermore, specific algorithms were more transferable between lakes than others, suggesting a possible ranking of algorithms could be established. Additional consideration should be placed on understanding why algorithms perform differently between lakes. In this study, the difference in accuracy of the algorithms, as determined by RMSE was expected to be a result in the differing water quality characteristics between the lakes as shown in Table 7 and Table 8 (USEPA 2012, Miltner 2018). . Given characteristics of Taylorsville's chlorophyll concentration, larger range and higher standard deviation, it is reasonable that the RMSE values at Taylorsville would be higher than those of the Harsha algorithms, whose condition at the time of sampling exhibited a narrower range of relatively high chlorophyll across the entire lake. Another potentially conflating factor influencing the performance of these algorithms is the variation in algal communities between the lakes. Harsha was almost completely dominated by cyanobacteria compared to Taylorsville that had 25% of its community comprised of taxa other than cyanobacteria. Further research is needed to quantify how overall chlorophyll concentrations and algal division dominance influence the efficacy of these algorithms.

Table 7

A comparison of the chlorophyll content between measured at the 44 surface observation points at Harsha Lake and the 70 observation points at Taylorsville Lake. Chlorophyll content was measured using SumReChl (section 2.4) in units of µg/L.

	Taylorsville Chlorophyll Concentrations	Harsha Chlorophyll Concentrations
Min	4.04	28.02
Max	130.56	85.63
Average	36.78	51.02
Range	126.52	57.62
STD	27.49	16.05

Table 8

A comparison of the algae taxonomy differences between Harsha Lake and Taylorsville Lake as described by algae divisions.

Algae Division	Taylorsville	Harsha
	Average Relative Abundance (%)	
Bacillariophyta	2.695	0.077
Chlorophyta	15.429	1.059
Chrysophyta	0.030	0.000
Cryptophyta	7.366	1.527

Cyanobacteria	72.443	97.320
Euglenophyta	0.068	0.000
Pyrrophyta	0.294	0.018
Total	98.325	100.000

The CASI algorithms performed well, overall, but it is not expected that these algorithms would be implemented in routine monitoring due to the high cost and intensive labor required for aircraft acquisition. Instead the CASI dataset was utilized as a baseline to study the portability of these algorithms under varying water quality conditions. On the other hand, Sentinel-2 a recently launched operational satellite had three potentially portable algorithms, which is encouraging for the consideration of operational remote sensing of HABs in inland lakes. The results demonstrated that the NDCI, 2BDA, and 3BDA algorithms were all portable across lakes with r^2 values all above 0.6. The NDCI and 2BDA algorithms were even higher with r^2 of greater than 0.7. Sentinel-2 is also likely be to a major contributing sensor in the detection and monitoring of HABs in small to mid-sized likes because the products are freely available through the ESA's data hub, the sensor has the appropriate spatial, and the Sentinel A/B constellation has a relatively quick return time of ~5-10 days (ESA, 2017).

WorldView-2 produced two portable algorithms, the 2BDA and NDCI, but there was a significant drop in the r^2 values from Harsha to Taylorsville. The 2BDA algorithm dropped from r^2 of 0.712 to 0.511 and the NDCI dropped from r^2 0.718 to 0.507 at Harsha and Taylorsville, respectively. Deeper investigation is needed to determine why this poor portability between lakes occurred for WorldView-2 significantly more than the other imagers.

Due to the unique configuration of band spacings on the Landsat-8 sensor, no algorithm was deemed portable. Furthermore, the best performing algorithms, the FLH Blue/Violet algorithms, demonstrated relatively poor correlations with r^2 values around 0.3. Given the results of this study it is not recommend that Landsat-8 imagery b small toe used for mid-sized inland lakes. The MODIS algorithms appear to have a limited use in the monitoring of chlorophyll-a as well, due to the combination of coarse spatial resolution and limited spectral bands in the regions associated with the important photosynthetic pigments.

Given the success of MERIS in previous studies (Augusto-Silva et al., 2014; Beck et al., 2016; Gower et al., 2008; Koponen et al., 2002), it was important to include this sensor in this study. Unfortunately, the coarse resolution of MERIS and the lake morphometry of Taylorsville only produced three water-only pixels, which was deemed too low for any reasonable quantitative conclusions. Although no evaluation of portability could be determined, the MERIS algorithms performed extremely well in Harsha lake with r^2 values greater than 0.8 for all algorithms except MCI. These results suggest that MERIS should be considered for all mid-sized to large water body monitoring, but difficult for the monitoring of small water bodies with sub-kilometer widths.

In general, the results of this study are promising but there are limitations and areas of concern. Signal to noise ratios are low in aquatic environments because most operational satellites were designed for terrestrial applications. This issue has been discussed at length in the literature, and there is general consensus that the application of these terrestrial satellites for inland water studies is still appropriate (Kallio, 2000; Kudela et al., 2015; Mishra and Mishra, 2012; Reif, 2011; Stumpf et al 2012; Stumpf et al., 2016). Stumpf et al. (2016) further addressed the many challenges of using remote sensing for mapping cyanotoxins, including biological, environmental, and even pigment detection methods. This paper follows that approach, by offering options in terms of sensor-algorithm pairs to better assist local decision makers. Even with these uncertainties and errors the results of this study demonstrate the ability to remotely sense water bodies to provide an estimated chlorophyll-a concentration. This is done by using the normalized chlorophyll-a indices and RMSE for the highest performing algorithm-imager combinations, which allow for similar prediction of chlorophyll-a values across algorithms and sensors (Table 4). For example, if a water manger determined that the threshold of concern for a particular water-body was a chlorophyll-a concentration of 50µg/L, this would correspond directly to the value of any normalized indices with a value of 50. This combined with that algorithm-sensor pairs RMSE would allow for a qualification of confidence in the measurement, so if the RMSE is 10, a value as low as 40 would be within the error range and that water-body could be considered near the threshold of concern. The RMSE's for the top performing algorithms in both lakes were under 15.

Overall, certain sensor-algorithm pairs correlate well enough with in-situ measurements of chlorophyll-a across differing that they would likely be considered useful for HAB monitoring effort in inland lakes. We think the model RMSE values were low enough to consider the accuracy of the algorithms high enough for HAB monitoring, where effect thresholds for chlorophyll-a are likely to be above 25 µg/L (USEPA 2012, Miltner 2018). The exact influences of water quality characteristics, such as algal division dominance and absolute chlorophyll concentration, on the performances of individual sensor-algorithm pairs are not yet fully understood and is an area ripe for future study. This study offered a unique comparison between lakes of the accuracy of chlorophyll estimates from hyperspectral imagery using twenty-nine sensor-algorithm pairs to determine which pairs appear most valuable for future monitoring of HABs. The increase in HAB extent and frequency has led to the need of multi-sensor networks, which require intense processing and cross-platform algorithms. This study has attempted to evaluate these algorithms across sensors and automate much of the procedures using scripts in R to provide closer to near real-time monitoring need for HAB monitoring and water quality management.

Author contributions

All authors played major roles in one of the most extensive coincident aircraft imaging, coincident surface observation and biogeochemical analysis campaigns for the evaluation of remote sensing algorithms for the estimation of water quality to date.

Acknowledgments

This study was funded by the U.S. Army Corps of Engineers. The U.S. Environmental Protection Agency and the Kentucky Department of Environmental Protection, Division of Water provided valuable in-kind services. Any use of trade, product, or firm names is for descriptive purposes only and does not imply endorsement by the U.S. Government. This article expresses only the personal views of the U.S. Army Corps of Engineers employees listed as authors and does not necessarily reflect the official positions of the Corps or of the Department of the Army.

References

Alawadi, F. (2010). Detection of surface algal blooms using the newly developed algorithm surface algal bloom index (SABI). Proceedings of SPIE, 7825. http://dx.doi.org/ 10.1117/12.862096.

Allee, R. J., & Johnson, J. E. (1999). Use of satellite imagery to estimate surface chlorophyll a and Secchi disc depth of Full Shoals Reservoir, Arkansas, USA. International Journal of Remote Sensing, 20, 1057–1072.

Augusto-Silva, P. B., Ogashawara, I., Barbosa, C. C. F., de Carvalho, L. A. S., Jorge, D. S. F., Fornari, C. I., & Stech, J. L. (2014). Analysis of MERIS reflectance algorithms for estimating chlorophyll-a concentration in a Brazilian Reservoir. Remote Sensing, 6, 11689–117077.

Backer L. C. (2002). Cyanobacterial harmful algal blooms: developing a public health response. Lake and reservoir Management, 18(1), 20-31.

Beck, R.A. and 22 others; Comparison of satellite reflectance algorithms for estimating chlorophyll-a in a temperate reservoir using coincident hyperspectral aircraft imagery and dense coincident surface observations, *Remote Sens. Environ.*, **2016**, *178*, 15-30.

Binding, C. E., Greenberg, T. A., & Bukata, R. P. (2013). The MERIS maximum chlorophyll index; its merits and limitations for inland water algal bloom monitoring. Journal of Great Lakes Research, 39, 100–107.

Blondeau-Patissier, D., Gower, J. F. R., Dekker, A. G., Phinn, S. R., & Brando, V. E. (2014). A review of ocean color remote sensing methods and statistical techniques for the detection, mapping and analysis of phytoplankton blooms in coastal and open oceans. Progress in Oceanography, 123, 123–144.

Brivio, P. A., Giardino, C., & Zilioli, E. (2001). Determination of chlorophyll concentration changes in Lake Garda using an image-based radiative transfer code for Landsat TM images. International Journal of Remote Sensing, 22, 487–502.

Cannizzaro, J. P., & Carder, K. L. (2006). Estimating chlorophyll a concentrations from remote-sensing reflectance in optically shallow waters. Remote Sensing of Environment, 101, 13–24.

Chipman, J. W., Olmanson, L. G., & Gitelson, A. A. (2009). Remote sensing methods for lake management: A guide for resource managers and decision-makers. Developed by the North American Lake Management Society in collaboration with Dartmouth College, University of Minnesota, and University of Nebraska for the United States Environmental Protection Agency.

Choubey, V. K. (1994). Monitoring water quality in reservoirs with IRS-1A-LISS-I. Water Resources Management, 8, 121–136.

Dall'Olmo, G., & Gitelson, A. A. (2005). Effect of bio-optical parameter variability on the remote estimation of chlorophyll-a concentration in turbid productive waters: Experimental results. Applied Optics, 44, 412–422.

Dall'Olmo, G., Gitelson, A. A., & Rundquist, D. C. (2003). Towards a unified approach for remote estimation of chlorophyll-a in both terrestrial vegetation and turbid productive waters. Geophysical Research Letters, 30, 1038. http://dx.doi.org/10.1029/ 2003GL018065.

Dekker, A. G., & Peters, S. W. (1993). The use of the thematic mapper for the analysis of Eutrophic Lakes: A case study in The Netherlands. International Journal of Remote Sensing, 14, 799–822.

Dokulil, M. T., And K. Teubner. 2000. Cyanobacterial dominance in lakes. Hydrobiologia 438: 1-12.

Ekstrand, S. (1992). Landsat TM based quantification of chlorophyll-a during algae blooms in coastal waters. International Journal of Remote Sensing, 13, 1913–1926.

European Space Agency (ESA). (2018, January 25). Missions: Sentinel-3 https://sentinels.copernicus.eu/web/sentinel/missions/sentinel-3

European Space Agency (ESA). (2017, September 20). Retrieved from Copernicus Open Access Hub: https://scihub.copernicus.e

Fraser, R. N. (1998). Hyperspectral remote sensing of turbidity and chlorophyll a among Nebraska Sand Hills lakes. International Journal of Remote Sensing, 19, 1579–1589.

Frohn, R. C., & Autrey, B. C. (2009). Water quality assessment in the Ohio River using new indices for turbidity and chlorophyll-a with Landsat-7 Imagery. Draft Internal Report, U.S. Environmental Protection Agency.

Gitelson, A. A. (1992). The peak near 700 nm on reflectance spectra of algae and water: Relationships of its magnitude and position with chlorophyll concentration. International Journal of Remote Sensing, 13, 3367–3373.

Gitelson, A. A., Garbuzov, G., Szilagyi, F., Mittenzwey, K. H., Karnieli, A., & Kaiser, A. (1993). Quantitative remote sensing methods for real-time monitoring of inland waters quality. International Journal of Remote Sensing, 14, 1269–1295.

Gitelson, A. A., Nikanorov, A. M., Sabo, G., & Szilagyi, F. (1986). Etude de la qualite des eaux de surface par teledetection, monitoring to detect changes in water quality series. Proceedings of the International Association of Hydrological Sciences, 157, 111–121.

Gitelson, A. A., Gritz, U., & Merzlyak, M. N. (2003). Relationships between leaf chlorophyll content and spectral reflectance and algorithms for non-destructive chlorophyll assessment in higher plant leaves. Journal of Plant Physiology, 160, 271–282.

Glasgow, H. B., Burkholder, J. M., Reed, R. E., Lewitus, A. J., & Kleinman, J. E. (2004). Realtime remote monitoring of water quality: A review of current applications, and advancements in sensor technology, telemetry, and computing technologies. Journal of Experimental Marine Biology and Ecology, 300, 409–448.

Gower, J., King, S., & Goncalves, P. (2008). Global monitoring of plankton blooms using MERIS MCI. International Journal of Remote Sensing, 29, 6209–6216.

Graham, J. L. (2006). Harmful algal blooms. USGS Fact Sheet, 2006-3147.

Han, L., Rundquist, D. C., Liu, L. L., Fraser, R. N., & Schalles, J. F. (1994). The spectral responses of algal chlorophyll in water with varying levels of suspended sediment. International Journal of Remote Sensing, 15, 3707–3718.

Hijmans, R. J. (2016). raster: Geographic Data Analysis and Modeling. R package version 2.5-8. https://CRAN.R-project.org/package=raster

Hu, C., Barnes, B. B., Qi, L., & Crcoran, A. A. (2015). A harmful algal bloom of Karenia brevis in the Northeastern Gulf of Mexico as revealed by MODIS and VIIRS: A comparison. Sensors, 15, 2873–2887.

Hunter, P. D., Tyler, A. N., Willby, N. J., & Gilvear, D. J. (2008). The spatial dynamics of vertical migration by Microcystis aeruginosa in a eutrophic shallow lake: A case study using high spatial resolution time-series airborne remote sensing. Limnology and Oceanography, 53, 2391–2406.

Johansen, R. A. (2017). Chlorophyll-a Detection and Value Extraction from Raster Imagery. GitHub repository. https://github.com/RAJohansen/Chlorophyll-a_Detection_Algorithms

Kallio, K. (2000). Remote sensing as a tool for monitoring lake water quality. In P. Heinonen, G. Ziglio, & A. van der Beken (Eds.), Hydrological and limnological aspects of lake monitoring (pp. 237–245). Chichester, England: John Wiley & Sons, Ltd.

Klemas, V. (2012). Remote sensing of algal blooms: An overview with case studies. Journal of Coastal Research, 28(1A), 34–43.

Kneubuhler, M., Frank, T., Kellenberger, T. W., Pasche, N., & Schmid, M. (2007). Mapping chlorophyll-a in Lake Kivu with remote sensing methods. Proceedings of the Envisat Symposium 2007, Montreux, Switzerland 23–27 April 2007 (ESA SP-636, July 2007).

Koponen, S., Pulliainen, J., Kallio, K., & Hallikainen, M. (2002). Lake water quality classification with airborne hyperspectral spectrometer and simulated MERIS data. Remote Sensing of Environment, 79, 51–59.

Kudela, R. M., Palacios, S. L., Austerberry, D. C., Accorsi, E. K., Guild, L. S., & Torres-Perez, J. (2015). Application of hyperspectral remote sensing to cyanobacterial blooms in inland waters. Remote Sensing of Environment, 1–10. http://dx.doi.org/10.1016/j.rse. 2015.01.025 (10 pp.).

Linkov, I., Satterstrom, F. K., Loney, D., & Steevans, J. A. (2009). The impact of harmful algal blooms on USACE operations. ANSRP technical notes collection. ERDC/TN ansrp-09-1. Vicksburg, MS: U.S. Army Engineer Research and Development Center.

Matthews, A. M., Duncan, A. G., & Davison, R. G. (2001). An assessment of validation techniques for estimating chlorophyll-a concentration from airborne multispectral imagery. International Journal of Remote Sensing, 22, 429–447.

Miltner, R.J. (2018). Eutrophication endpoints for large rivers in Ohio, USA. Environmental Monitoring and Assessment. 190:55. DOI: 10.1007/s10661-017-6422-4)

Mishra, S., & Mishra, D. R. (2012). Normalized difference chlorophyll index: A novel model for remote estimation of chlorophyll-a concentration in turbid productive waters. Remote Sensing of Environment, 117, 394–406.

Mittenzwey, K. -H., Ulrich, S., Gitelson, A.-. A., & Kondratiev, K. Y. (1992). Determination of chlorophyll a of inland waters on the basis of spectral reflectance. Limnology and Oceanography, 37, 147–149.

Morel, A., & Prieur, L. (1977). Analysis of variation in ocean color. Limnology and Oceanography, 22, 709–722.

Peltzer, E. T. (2015). Model 1 and model 2 regressions. http://www.mbari.org/staff/etp3/ regress.htm (Last updated 18 May 2009, last accessed, 27 April 2015).

Picard, Richard; Cook, Dennis (1984). "Cross-Validation of Regression Models". *Journal of the American Statistical Association*. **79** (387): 575–583.

Pinero, G., Perelman, S., Guerschman, J. P., & Paruleo, J. M. (2008). How to evaluate models: Observed vs. predicted or predicted vs. observed. Ecological Modelling, 216, 316–322.

Pitois, S., Jackson, M. H., & Wood, B. J. B. (2000). Problems associated with the presence of cyanobacteria in recreational and drinking waters. *International Journal of Environmental Health Research*, *10*(3), 203-218.

Ohio Department of Health, 2017. Harmful Algal Blooms: Implications for Tap/Drinking Water and Recreational Waters. url: https://www.odh.ohio.gov/odhprograms/eh/HABs/algalblooms.aspx. Updated 8/8/2017.

Quibell, G. (1992). Estimation of chlorophyll concentrations using upwelling radiance from different freshwater algal genera. International Journal of Remote Sensing, 13, 2611–2621.

R Core Team (2017). R: A language and environment for statistical computing. R Foundation for Statistical Computing, Vienna, Austria. URL https://www.R-project.org/.

Reif, M. (2011). Remote sensing for inland water quality monitoring: A U.S. Army Corps of Engineers Perspective. Engineer Research and Development Center/Environmental Laboratory Technical Report (ERDC/EL TR)-11–13 (44 pp.).

Rundquist, D. C., Han, L., Schalles, J. F., & Peake, J. S. (1996). Remote measurement of algal chlorophyll in surface waters: The case for the first derivative of reflectance near 690 nm. Photogrammetric Engineering and Remote Sensing, 62, 195–200.

Sauer, M. J., Roesler, C. S., Werdell, P. J., & Barnard, A. (2012). Under the hood of satellite empirical chlorophyll a algorithms: Revealing the dependencies of maximum band ratio algorithms on inherent optical properties. Optics Express, 20, 1–15.

Sawaya, K. E., Olmanson, L. G., Heinert, N. J., Brezonik, P. L., & Bauer, M. E. (2003). Extending satellite remote sensing to local scales: land and water resource monitoring using high-resolution imagery. Remote Sensing of Environment, 88(1–2), 144–156.

Schalles, J. F., Schiebe, F. R., Starks, P. J., & Troeger, W. W. (1997). Estimation of algal and suspended sediment loads (singly and combined) using hyperspectral sensors and integrated mesocosm experiments. Proc. Fourth Int. Conf. Remote Sensing Mar. Coastal Environ., 17–19 March 1997, Orlando, Florida, 1. (pp. 247–258). Ann Arbor: Environmental Research Institute of Michigan.

Shen, L., Xu, H., & Guo, X. (2012). Satellite remote sensing of harmful algal blooms (HABs) and a potential synthesized framework. Sensors, 12, 7778–7803.

Stone, M. (1974) "Cross-Validatory Choice and Assessment of Statistical Predictions," Journal of the Royal Statistical Society, Vol. 36, No. 1, pp. 111-147.

Stumpf, R. P., & Tomlinson, M. (2005). Remote sensing of harmful algal blooms. Remote sensing of coastal Aquatic environments. Springer, 277–296.

Stumpf, R. P., Wynne, T. T., Baker, D. B., & Fahnenstiel, G. L. (2012). Interannual variability of cyanobacterial blooms in Lake Erie. PloS One, 7, 1–11.

Stumpf, R. P., Davis, T. W., Wynne, T.T., Graham, J. L., Loftin, K. A., Johengen, T. H., Gossiaux, D., Palladino, D., Burtner, A. (2016) Challenges for mapping cyanotoxin patterns from remote sensing of cyanobacteria. Harmful Algae. 54, 160-173.

Thiemann, S. T., & Kaufmann, H. (2002). Lake water quality monitoring using hyperspectral airborne data - A semiempirical multisensor and multitemporal approach for the Mecklenburg Lake District, Germany. Remote Sensing of Environment, 81, 228–237.

Thonfeld, F., Feilhauer, H., & Menz, G. (2012). Simulation of Sentinel-2 images from hyperspectral data. Proceedings European Space Agency Conference (http://www. congrexprojects.com/docs/12c04_docs2/poster2_43_thonfeld.pdf).

U.S. Environmental Protection Agency (USEPA) (2000). Ambient Water Quality Criteria Recommendations: Lakes and Reservoirs in Nutrient Ecoregion VI (EPA 822-B-00-008).

U.S. Environmental Protection Agency (USEPA) (2012). Cyanobacteria and cyanotoxins: Information for drinking water systems. U.S. Environmental Protection Agency, Office of Water (EPA-810F11001).

U.S. Geological Survey (2015). Landsat-8 (L8) Data Users Handbook, 1–98.

Verdin, J. P. (1985). Monitoring water quality conditions in a large western reservoir with Landsat imagery. Photogrammetric Engineering and Remote Sensing, 51, 343–353.

Veryla, D. L. (1995). Satellite remote sensing of natural resources. CRC Lewis (199 pp.).

Vos, W. L., Donze, M., & Bueteveld, H. (1986). On the reflectance spectrum of algae in water: The nature of the peak at 700 nm and its shift with varying concentration. Tech. Report, Communication on Sanitary Engineering and Water Management, Delft, The Netherlands 86–22.

Wang, Y., Xia, H., Fu, J., & Sheng, G. (2004). Water quality change in reservoirs of Shenzen, China: Detection using Landsat/TM data. The Science of the Total Environment, 328, 195–206.

World Health Organization (WHO). (2003). *Cyanobacterial toxins: Microcystin-LR in Drinking-water.* Geneva, Switzerland: World Health

World Health Organization (WHO). (1999). Toxic Cyanobacteria in Water: A guide to their public health consequences, monitoring and management. London, England. St. Edmundsbury Press.

Wynne, T. T., Stumpf, R. P., Tomlinson, M. C., & Dyble, J. (2012). Characterizing a cyanobacterial bloom in western Lake Erie using satellite imagery and meteorological data. Limnology and Oceanography, 55, 2025–2036.

Zhao, D. Z., Xing, X. G., Liu, Y. G., Yang, J. H., & Wang, L. (2010). The relation of chlorophylla concentration with the reflectance peak near 700 nm in algae-dominated waters and sensitivity of fluorescence algorithms for detecting algal bloom. International Journal of Remote Sensing, 31, 39–48.